The 4th European sCO2 Conference for Energy Systems
March 23-24, 2021, Online Conference

2021-sCO2.eu-120

PRELIMINARY AERODYNAMIC DESIGN OF A SUPERCRITICAL CARBON DIOXIDE COMPRESSOR IMPELLER FOR WASTE HEAT RECOVERY APPLICATIONS

Shantanu Thada*
Dept. of Mechanical Engineering,
Indian Institute of Technology Bombay
Mumbai, India

A M Pradeep
Dept. of Aerospace Engineering,
Indian Institute of Technology Bombay
Mumbai, India

Arunkumar Sridharan
Dept. of Mechanical Engineering,
Indian Institute of Technology Bombay
Mumbai, India

ABSTRACT

Supercritical Carbon dioxide (S-CO_2) Brayton cycles have garnered significant attention in the recent past as an alternative source for renewable energy. The present research provides a simplistic, yet robust methodology to appropriately size and design the impeller of a centrifugal compressor for a 12.5 MW_e waste heat recovery S-CO_2 power plant. Two prominent variants of the S-CO_2 cycle are studied and optimized with the aim of maximizing the power output using genetic algorithm. To calculate the geometry from the inlet and exit thermodynamic conditions of the optimized cycle, conservation equations are solved. The impeller is sized and a brief study on condensation in the impeller throat is performed. The effect of multi-staging on condensation is investigated. Further, the performance model is coupled with the design scheme to dynamically modify the impeller geometry. Using the developed model, the geometrical parameters of the S-CO_2 impeller are calculated. In addition to the geometry, certain impeller performance parameters are reported and are observed to lie within the permissible limits.

INTRODUCTION

Advancements in the technology of power generation have undergone significant growth in the past two centuries. Although the fundamental principle of electricity generation remains unchanged, technologies of heat-to-power conversion have evolved with a straightforward goal of improving the process efficiency as well as production capacity. In the year 2018, primary energy consumption has grown fastest since 2010 at a rate of 2.9%, doubling its 10-year average of 1.5% per annum **[1]**. The use of fossil fuels to generate power has brought large-scale industrialization. However, the problem of climate change has provided a push towards the innovation of renewable technologies for power generation.

Along with the use of renewables, re-using the waste heat produced by the various industrial sectors improves the overall thermodynamic efficiency of the process. The process of re-using waste heat from exhaust streams to produce power is referred to as waste heat recovery (WHR) in this study. Recovery of waste heat is known to have benefits such as reduction in fuel/energy consumption cost, reduction in pollution, increment in process efficiency, and a smaller power block **[2]**. Waste heat recovery has applications in energy intensive industries such as the metal industry (Iron, Aluminum, Steel), Glass, Paper, and Cement manufacturing industries. Waste heat source are classified based on the source temperature, primarily into three categories: High (>600˚C), Medium (250˚C - 600˚C) and Low (<250˚C) **[3]**. For medium-to-low heat source temperatures, the challenges involved with installing a WHR unit includes the presence of low-quality heat source, the capital cost for installation and the maintenance costs.

Among the different options for generating power from a waste-heat source, the supercritical Carbon dioxide Brayton cycle offers higher cycle efficiency at lower temperatures, reduced power block and wide range of operational temperatures. The concept of CO_2 being used as a working fluid for power generation was first introduced when Sulzer Ltd. filed a patent **[4]** for a partial condensation CO_2 Brayton reactor in 1948. Feher in 1968 **[5],** proposed the first simple recuperated Brayton cycle (RC) configuration. Feher reported that the designed configuration is advantageous as it provides higher thermal efficiency, no turbine blade erosion, no pump cavitation, low volume to power ratio, single stage turbine and pump. Another prominent S-CO_2 cycle configuration known as the recuperated recompression Brayton cycle (RRC) was proposed by Angelino in 1968 **[6]**. The RRC configuration has a smaller precooler size due to lower CO_2 mass flow rate as well as a lower pinch point in Low Temperature Recuperator (LTR), thereby increasing the cycle thermal efficiency. The

* corresponding author(s)
Email: s.thada@gmail.com

DOI: 10.17185/duepublico/73958

schematic of the RC and RRC configurations are presented in Figure 1 and 2 respectively.

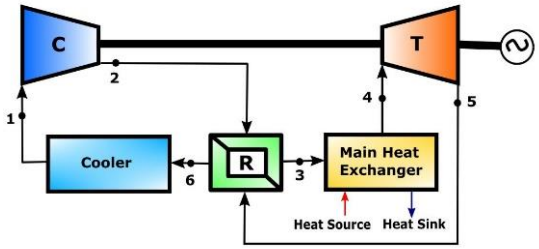

Figure 1: Schematic of the S-CO_2 RC configuration

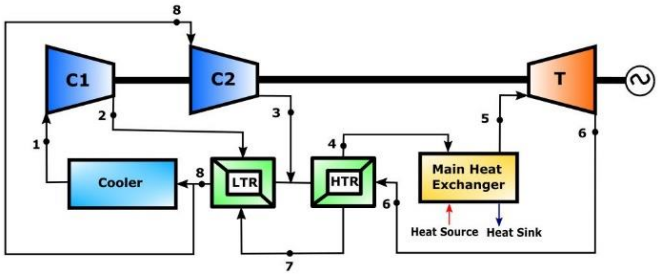

Figure 2: Schematic of the S-CO_2 RRC configuration

For a supercritical cycle, the compression process occurs close to the supercritical point which introduces certain challenges in its design. Turbomachinery for S-CO_2 has a variety of problems related to local condensation, corrosion and losses associated with them. Typically, three types of losses may occur due to condensation: kinematic relaxation loss, thermodynamic wetness loss and breaking loss, which needs to be properly assessed **[7]**. Strong variations in properties near the critical point restricts the use of empirical loss correlations developed for conventional air-based turbomachinery. Specifically, in the compressor, the impeller is the one of the few rotating parts that further complicates the design process. The design methodology for an S-CO_2 compressor needs to be appropriately modified to deal with these challenges.

Conventional air-based design methodology for generating the geometry of a centrifugal compressor requires certain modifications to account for the above stated challenges for unconventional fluids. The present study addresses the literature gap of turbomachinery design for non-ideal working fluids, specifically, CO_2 in supercritical state. The primary objective of the study is to develop a geometry of a centrifugal compressor impeller for a waste heat recovery (WHR) S-CO_2 power plant for industrial applications. A preliminary design methodology is developed to calculate the geometrical parameters of a centrifugal compressor based on the thermodynamic cycle parameters. To achieve this, first, two prominent configurations of the S-CO_2 cycle are thermodynamically optimized using genetic algorithm methodology for a defined waste-heat source.

CYCLE DESIGN AND OPTIMIZATION

As identified in Wright et al. **[8]**, one of the first commercial applications for S-CO_2 power systems is likely to be 5-20 MWe Waste Heat Recovery (WHR) power systems for industrial applications (particularly steel mills, cement plants). The present study focuses on developing a S-CO_2 cycle for WHR with a power generation capacity of 12.5 MWe. The waste-heat source is designed based on studying the exhaust gas characteristics of various small to medium scale plants in the cement industry **[9]**. The characteristics of the flue gases generated from the heat source are provided in Table 1. The cooler air exhaust temperature in a cement plant typically lies in the range of 400°C - 450°C with a mass flow rate equal to 50kg/s for a 1 MTPA clinker production capacity.

Based on the inputs provided, various configurations of the S-CO_2 cycles are explored. Since the idea is to use a waste-heat source, it is important to design a power conversion system that delivers the maximum net power output. Calculations are performed using codes written on MATLAB R2018a **[10]** with the CoolProp **[11]** add-on to calculate the properties of Carbon dioxide based on Span & Wagner equation of state. The governing equations for every component of the thermodynamic cycle are based on the solution of steady-state mass, momentum and energy balance.

Table 1: Exhaust Gas Characteristics of the Waste-Heat Source

Working Fluid	Air
Inlet Temperature of Exhaust Gas	450°C
Inlet Pressure of Exhaust Gas	1 atm
Mass Flow Rate of Exhaust Gas	50 kg/sec
Ambient Temperature	25°C

Thermodynamic Cycle Modelling

Primary components of an S-CO_2 Brayton cycle comprise of compressor(s), turbine, source heat exchanger, cooler and recuperator(s). Along with the schematics, the cycle states for RC and RRC configuration are numbered in the schematics presented in Figure 1 and 2, respectively. Thermodynamic model of these components is based on conversation equations of mass and energy. Energy balance across the main heat exchanger for RC configuration is depicted in Equation 1, while the enthalpy balance across the recuperator is depicted in Equation 2. In the model, input parameters such as the compressor efficiency, turbine efficiency and fractional pressure drop in heat exchangers are assumed to be constant. Primary inputs to the model are the design variables, which outputs the remaining states at the entry and exit of each component. For the RC configuration, the design variables include the compressor inlet pressure, compressor exit pressure, compressor inlet temperature, mass flow rate and terminal temperature difference. The RRC configuration includes an additional design variable other than the design variables of the RC configuration, i.e., the main compressor mass flow fraction. Using the thermodynamic states obtained from the model,

performance parameters such as the thermal efficiency and net power output are calculated. In the heat exchangers, it has been observed in multiple studies like Mohagheghi et. al **[12]**, Khadse et. al **[13],** that the pinch point lies at the cold end of the recuperator. Terminal temperature difference at the cold end of the recuperator is an input parameter to the model, and is assumed equal to the pinch point.

$$\dot{m}_{air} \times (h_{entry} - h_{exit}) = \dot{m}_{CO_2} \times (h_4 - h_3) \quad (1)$$

$$h_3 - h_2 = h_5 - h_6 \quad (2)$$

Optimization Methodology

A thermodynamic cycle optimization consists of obtaining a set of input design variables that maximizes the performance parameter(s). Certain constraints are imposed during this optimization to ensure that the mass, momentum and energy conservation are not violated. In this study, Genetic Algorithm (GA) is used to perform the optimization. As stated by Mitchell **[14]**, GA is an optimization algorithm based on a nature-based selection process which imitates the biological evolution, using the bio-inspired operators such as mutation, crossover and selection.

In a typical optimization process, derivative-based techniques are used to find the minimum of a defined function. However, for any function that has several local optimum points, it is likely that the technique results into capturing the local and not the global optimum. In contrast to the gradient based technique, GA does not require any analytical relations governing the system, it treats the system as a black box **[12]**. Here, a pre-defined waste heat source is available for waste-heat to power conversion, and the objective is to generate the maximum net power output from the available resource. Therefore, for this study, the objective function is the net power output of the S-CO_2 cycle. The iterative methodology followed by the Genetic Algorithm can be summarized in five steps:

1. Generate a random population of individuals. The individual's identity is determined using a set value of the decision variables.
2. Evaluate the fitness function for each individual. The fittest individuals, with greater values of fitness function are selected as parents to reproduce the next generation.
3. Create a new population using the fundamental rules of genetics inclusive of crossover, mutation and selection, with same number of individuals as in the previous generation.
4. Use the newly generated population to iterate the process of evaluation of fitness function, selection of fittest individuals and application of crossover, mutation and selection.
5. Repeat the iterative process until the best individual does not change its value for several generations i.e., until convergence is obtained.

Since the adopted methodology of GA for optimization is a stochastic technique, it is possible that at the end of the first run, the optimized minimum value differs slightly. Therefore, in some studies like Khadse et. al **[13]**, a sensitivity analysis is performed where the bounds of decision variables are narrowed down and the optimization is further performed to capture the optimal value. In the present study for all practical purposes, the value obtained at the end of first run can be used for further analysis, as it sufficiently captures the minima with good accuracy.

Assumptions and Input Parameters

Certain inherent assumptions are made during the modelling of the different S-CO_2 cycle configurations. Firstly, it is assumed that there are negligible heat losses occurring in the recuperators and main heat exchanger. Secondly, the involved turbo-machineries have a constant adiabatic efficiency throughout the operation. Thirdly, the working fluid CO_2, operates in steady state. For the present study, the compressor efficiency is set to 70% while the turbine efficiency is set to 85%. To model the pressure-drop in the heat exchangers, a fractional pressure drop coefficient is used as suggested by Angelino **[6]**, Mohagheghi and Kapat **[12]** and Khadse et. al **[13]**. For all heat exchangers involved in the cycles, the pressure drop is set to 2% of the inlet pressure.

For all practical purposes, the lower and upper bounds of the design variables are fixed, based on certain thermodynamic as well as material strength limitations. To avoid any occurrence of condensation, the lower limit of the compressor inlet temperature is set to 310 K, a value higher than the critical temperature of CO_2 (304.13 K). The lower limit of the compressor inlet pressure is fixed as 75 bar, which is higher than the critical pressure of CO_2. The higher limit of the compressor exit pressure is set to 330 bar due to the constraint of the structural capacity of the heat exchangers. State-of-the-art printed circuit heat exchangers are designed to operate at 250 to 350 bar **[13]** and hence the highest pressure of the cycle is limited by the structural performance of its components. The bounds of all the design variables for RC and RRC configuration are presented in Table 2 and Table 3 respectively.

Table 2: Input Bounds for the RC configuration

Design Variables for RC configuration	Lower Limit	Upper Limit
Compressor Inlet Pressure, P_1 (bar)	74	100
Compressor Exit Pressure, P_2 (bar)	120	330
Compressor Inlet Temperature, T_1 (K)	310	420
Mass Flow Rate of CO_2, $\dot{m}_{CO_2}$ (kg/s)	20	100
Terminal Temperature Difference, ΔT_{ttd} (K)	10	40

Table 3: Input Bounds for the RRC configuration

Design Variables for RRC configuration	Lower Limit	Upper Limit
Compressor Inlet Pressure, P_1 (bar)	74	100
Compressor Exit Pressure, P_2 (bar)	120	330
Compressor Inlet Temperature, T_1 (K)	310	420
Mass Flow Rate of CO_2, $\dot{m}_{CO_2}$ (kg/s)	20	100
Terminal Temperature Difference, ΔT_{ttd} (K)	10	40
Main Compressor (C1) Mass Flow to Total Mass Flow Fraction, f	0	1

Optimization Results

Providing the initial inputs listed above, the algorithm is run for 100 generations. For a successful run of the optimization process of the RC configuration, it is observed that the best performing individual is with a power-output value, $\dot{W}_{net}$ = 3.13 MW. For the best performing individual, optimized values of the design variables and T-s Diagram of RC configuration are listed in Table 4 and Figure 3, respectively. For the optimized RC configuration, the turbine inlet temperature is 666.23 K. It is noted that approximately 56% of the total heat available in the waste-heat source is utilized. The thermal efficiency of the optimized cycle is 25.09%. As presented in Table 5, for the optimized RRC configuration, it is observed that the mass flow fraction through the main compressor approaches the value equal to 1. This is in agreement with Mohagheghi's study **[12]**, which states that for lower CO_2 to exhaust gas stream mass flow rates, the RRC configuration approaches the RC configuration. Therefore, no significant advantage of splitting the mass flow rate is observed in the RRC configuration.

Table 4: Optimized Design Variables of RC Configuration

Optimized Design Variables for RC Configuration	Values
Compressor Inlet Pressure, $\boldsymbol{P_1}$ (bar)	88.44
Compressor Exit Pressure, $\boldsymbol{P_2}$ (bar)	307.59
Compressor Inlet Temperature, $\boldsymbol{T_1}$ (K)	310.13
Mass Flow Rate of CO_2, $\boldsymbol{\dot{m}_{CO_2}}$ (kg/s)	48.76
Terminal Temperature Difference, $\boldsymbol{\Delta T_{ttd}}$ (K)	10
Net Power Output of the Cycle, $\boldsymbol{\dot{W}_{net}}$ (MW)	3.13

Table 5: Optimized Design Variables of RRC Configuration

Optimized Design Variables for RC Configuration	Values
Compressor Inlet Pressure, $\boldsymbol{P_1}$ (bar)	92.88
Compressor Exit Pressure, $\boldsymbol{P_2}$ (bar)	303.00
Compressor Inlet Temperature, $\boldsymbol{T_1}$ (K)	310
Mass Flow Rate of CO_2, $\boldsymbol{\dot{m}_{CO_2}}$ (kg/s)	48.17
Terminal Temperature Difference, $\boldsymbol{\Delta T_{ttd}}$ (K)	10.4
Main Compressor Mass Flow Fraction, f	1
Net Power Output of the Cycle, $\boldsymbol{\dot{W}_{net}}$ (MW)	2.94

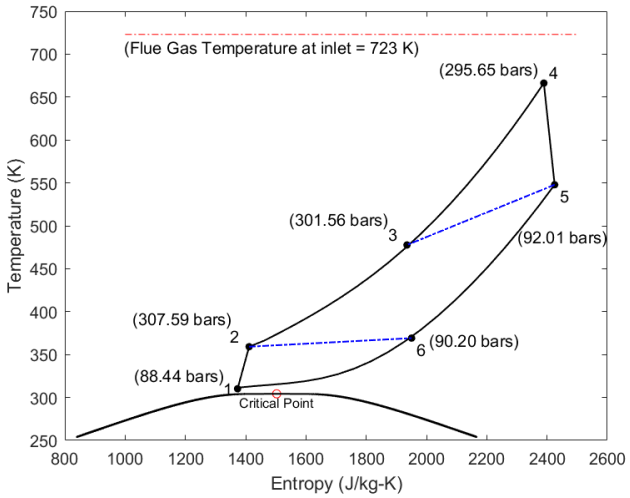

Figure 3: T-s Diagram of the optimized RC configuration

COMPRESSION SYSTEM DESIGN

Supercritical CO_2 Brayton cycles are characterized by relatively high operational pressures and moderate operational temperatures. Being in the proximity of critical point, the density of working fluid is high and hence the cycle components are compact. The volumetric flows in turbomachinery are low and hence even for high power outputs in the range of 5-10 MWe, centrifugal compressors can be employed. Using non-dimensional scaling, the size of turbomachinery is estimated from the desired power output **[15]**. In addition to the complexities involved non-ideal fluid modelling and simulation, the rotational motion of the impeller of a centrifugal compressor introduces additional complexity in the design process. The present study focuses on the preliminary aerodynamic design of a centrifugal compressor impeller for the optimized RC configuration. For the optimized cycle, the total-to-total pressure ratio of the compressor is 3.478. Typically, centrifugal compressors are expected to deliver a pressure ratio close to four in a single stage, hence, it is likely to achieve the pressure rise for the optimized cycle in a single stage. The isentropic efficiency assumed for the compressor is 0.7.

Initial Sizing

The methodology of conventional air-based turbomachinery sizing using Balje's Diagram **[16]** has been adopted in the past literature such as Fuller et al. **[17]** and Monje et al. **[18]**. Contours of compressor efficiencies are plotted against the specific speed (Ns) and specific diameter (Ds) for different types of turbomachinery, as defined in Equations 3 and 4, respectively.

$$N_s = \frac{\omega \times \dot{V}^{0.5}}{\Delta h_s^{0.75}} \quad (3)$$

$$D_s = \frac{d \times \Delta h_s^{0.25}}{\dot{V}^{0.5}} \quad (4)$$

First, it is assumed that the compression process occurs in a single stage. The inlet and exit (isentropic and actual) properties are calculated assuming the compressor efficiency to be 0.7. From the thermodynamic entry and exit states of the compressor, the isentropic enthalpy rise and volume flow rate are calculated. For the specific speed, optimum value is identified to lie in the range of 0.6-0.75 as established in Monje et al. **[18]**. Inserting the optimum value of Ns in Equation 3, the RPM is calculated. Further, the resulting value of specific diameter is calculated using Balje's diagram. Value of the obtained Ds is plugged into Equation 4 to obtain the impeller diameter. For a single stage, the resulting diameter for the impeller comes out to be 0.102 m while the resulting RPM has a value of 47460.

The calculations performed above establish that the S-CO_2 turbomachinery components are relatively small in size due to high density of the working fluid. Smaller turbomachinery components typically operated on high RPM (>10000) to accommodate the required mass flow rate. According to Fuller **[17]**, there are several disadvantages of high RPM, including reduced life, higher maintenance costs and higher risk of condensation in the impeller throat. If the RPM is to be kept low, the compression might result into a multi-stage process. Additionally, the problem of condensation needs to be addressed for a single as well as a multi-stage S-CO_2 compressor. Therefore, to study the effects of multi-staging on condensation, the compression process is split into two stages. For the two-stage compression process, the specific enthalpy rise is divided into two equal parts and the impeller diameter and RPM are calculated using equations 3 and 4.

To quantify the phenomenon of condensation, a Mach number termed as "Acceleration Margin to Condensation" (AMC) is defined by Brenes **[18]** and shown in Equation 5. If the throat Mach number is greater than the AMC, it is assumed that the fluid at the impeller throat has accelerated into the two-phase dome and therefore condensation has occurred.

$$M_{AMC} = \frac{C_{sat}}{a_{sat}} = \frac{\sqrt{2 \times \left(h_{o1} - h(s_{sat}, T_{sat})\right)}}{a(s_{sat}, T_{sat})} \quad (5)$$

The choice of the hub and tip radius, to calculate the throat mach number, is not based on a fixed methodology, and is in-fact based on diffusion constraints in the impeller as well as structural constraints of the shaft. Therefore, imposing a structural constraint on the shaft, the value of minimum shaft diameter is calculated using Equation 6, as stated by Loewenthal **[19]**. Typically, the material used for the shaft of a centrifugal compressor is Al S I 4330 **[20]**. Using the shear modulus of this material and previously assumed isentropic efficiency of the compressor as 70%, the minimum diameter comes out to be 3.44 mm. Therefore, any value above the minimum diameter can be considered.

$$d_{axis,minimum} = \sqrt[3]{\frac{16 \times \dot{W}_m}{\omega \times \pi \times \tau_m}} \quad (6)$$

Now, an iterative method is adopted to calculate the throat Mach number for each stage. The value of impeller inlet hub radius is fixed based on the above structural constraint and a safety factor. The value of tip radius at the inlet is varied such that it remains higher than the hub radius and lower than the impeller exit radius. Using the inlet hub radius, inlet tip radius, inlet stagnation conditions and the RPM, the area at impeller inlet is calculated and the velocity diagram is solved by invoking the continuity equation. Assuming isentropic flow and equating the stagnation properties, static properties at the impeller throat are calculated and the velocity triangle is solved. The absolute and relative velocity at the throat along with the static thermodynamic properties are used to calculate the throat mach number. The throat area is calculated as depicted in Figure 4. The results are plotted graphically in Figure 5 and 6 for the single and two-stage compressors with hub radius set to a value of 7.525 mm for both cases. The value of hub radius is set assuming a sufficient factor of safety, in this particular scenario, equivalent to 4.5.

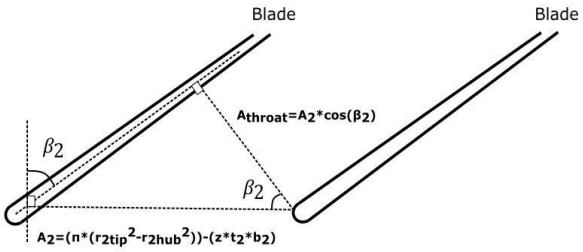

Figure 4: Area Calculation for Impeller Throat

It should be noted that in Figure 5 for the single-stage compressor, for tip radius more than 0.035 m, relative Mach number at throat is higher than the AMC and therefore, condensation might occur. Therefore, for a single stage compressor, tip radius less than 0.03 m should be selected. For the first stage of the two-stage (Figure 6), the value of relative and absolute Mach number remains less than AMC for all values of the tip radius. This is because the RPM, and therefore the Mach numbers of the multi-stage compressors are low. However, since multi-stage compression process leads to additional component costs and the single stage compressor does not show any condensation below a certain tip radius, the single stage compression process is selected.

Based on the condensation analysis, the inlet hub radius and inlet tip radius values are selected to be equal to 7.525 mm and 21.5 mm respectively. The resulting hub-to-tip ratio for the compressor is 0.35. Few other parameters, such as the number

of blades, thickness of each blade and clearance gap are chosen by the user based on prior design experience.

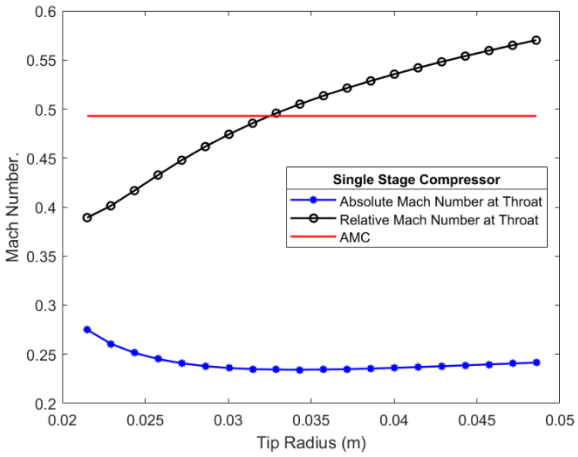

Figure 5: Absolute and Relative Mach Number at Throat for a Single Stage Compressor

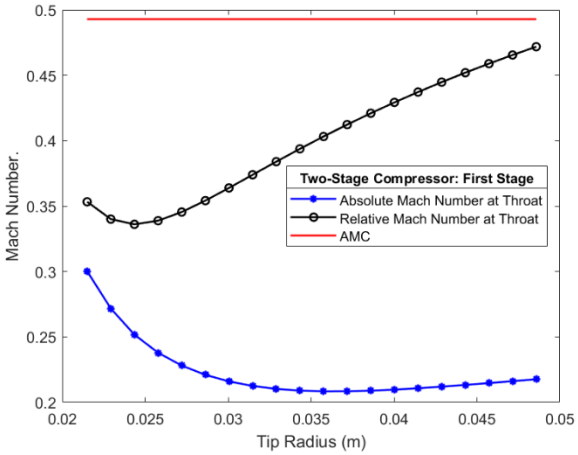

Figure 6: Absolute and Relative Mach Number at Throat for First Stage of Two-Stage Compressor

Methodology of Inverse Design

The methodology of inverse design consists of obtaining the geometry of the compressor from the inlet and exit stagnation properties, mass flow rate and RPM. A modified version of the inverse design methodology developed by Brenes **[18]** is adopted in the present work. To obtain the geometry of a S-CO_2 centrifugal compressor impeller, a computerized preliminary inverse design process is developed in this section. A set of operating conditions, listed below, is provided to the program and conservation equations of mass, momentum and energy are solved to calculate the geometrical parameters.

1. Total thermodynamic conditions at inlet and exit
2. Mass flow rate
3. RPM of the impeller
4. Hub and shroud diameters at impeller inlet
5. Tip diameter at impeller exit
6. Equation of State for working fluid

This preliminary design program is directly interfaced with the aerodynamic performance analysis tool adopted from Aungier's work **[21]**, to dynamically modify the geometry and enhance performance. The performance analysis tool takes in the inlet thermodynamic conditions, mass flow rate, RPM and compressor geometry as the input, and outputs the exit thermodynamic conditions. The program is developed in MATLAB **[10]** with CoolProp **[11]** add-on. This performance analysis tool is validated using experimental data published by the Sandia National Labs **[22]**. The geometrical parameters of the impeller are provided by Wright et. al. **[22]** and Vilim **[23]**. Static pressure at the impeller exit is compared to the experimental value, presented in Table 6. Given the complexity of the model, a mean deviation of 4.7% with a peak of 7% for the static pressure at the impeller exit seems satisfactory.

Table 6: Comparison of Experimental and Analytical Performance for the S-CO_2 Impeller

ω (RPM)	T_{o1} (K)	P_{o1} (bar)	$\dot{m}$ (kg/sec)	P_3 (exp.) (bar)	P_3 (mod.) (bar)	Error (%)
10000	305.5	76.76	0.45	76.76	77.614	1.11
20000	305.5	76.76	0.77	78.54	81.98	4.38
49000	306.3	78.54	1.82	94.25	98.13	4.12
60000	306.9	79.97	2.22	102.11	109.21	6.95
64900	307.9	82.11	2.41	108.53	116.17	7.04

The flow is solved at the inlet and exit of different sections of inducer and impeller. At each station of the compressor, the thermodynamic properties and velocity triangles are deduced, which in turn outputs the geometrical parameters of the compressor. For the present study, the calculation is performed at the inducer inlet, inducer exit or impeller inlet, impeller throat and impeller exit. Figure 7 highlights the different stations of a centrifugal compressor.

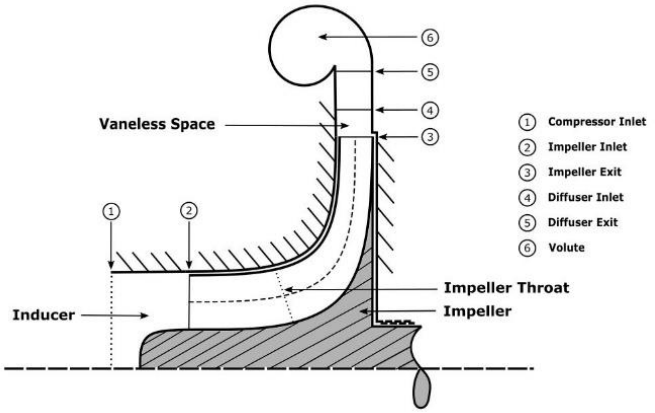

Figure 7: Highlighted Stations of a Centrifugal Compressor

Inducer Design

The primary target of the inducer design methodology is to evaluate the velocity triangle at the inlet to the inducer and set the blade metal angle equal to the relative velocity angle with the meridional direction, thereby assuming null incidence. The iterative algorithm is initialized assuming no losses. Using the inputs provided, the static properties and further, the velocity triangles are calculated at different stations. The relative flow angle at the inducer exit is set to the blade metal angle. At the throat, it is ensured that the absolute and relative mach numbers remain lower than AMC, to avoid any condensation. Using the obtained blade metal angle, the performance analysis tool for inducer calculates the total exit pressure at the inducer exit or impeller inlet. The algorithm for inducer design is highlighted in Figure 8.

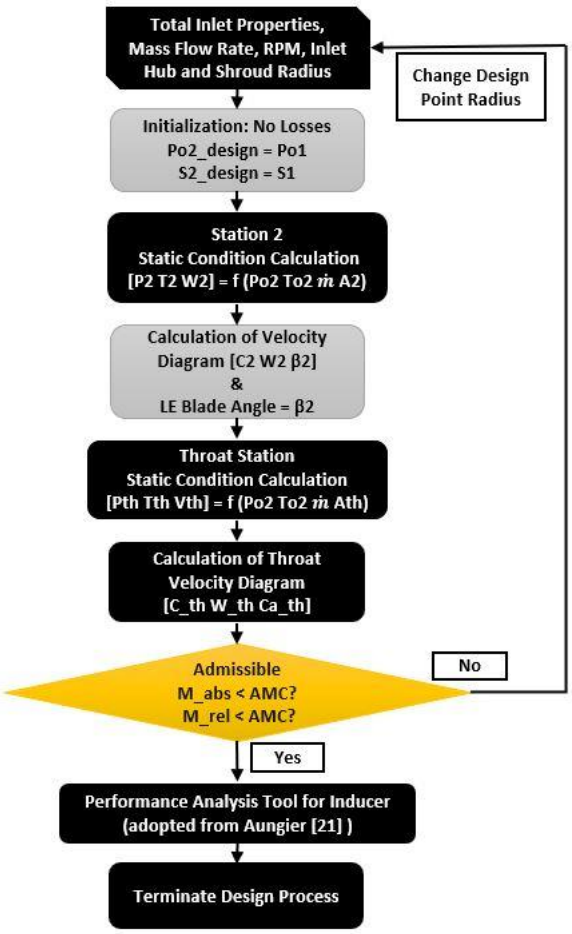

Figure 8: Algorithm for the Inducer Design

Impeller Design

The exit conditions of the inducer obtained from the inducer simulation are used to initiate the design process of the impeller. The focus of the design process for the impeller is to solve the velocity triangle at the impeller exit for which the desired pressure ratio is achieved (P_{o6}/P_{o1}). Along with this, performance parameters such as the slip and distortion factor are also calculated. It is known that certain losses occur in the static components of a compressor i.e., diffuser and volute. Prior to obtaining the performance of the compressor, an estimate of these losses is to be made and incorporated in the design process. Similarly, the isentropic efficiency is guessed to initiate the design process.

Losses in the diffuser and volute, $\kappa_{diff-vol}$ are assumed to be of a constant value during the design process of impeller. Using this term, the total pressure at the exit of the impeller is calculated. For the present study, the value of $\kappa_{diff-vol}$ is assumed to be 1%. The exit pressure of the compressor, P_{o6}, is calculated from the compressor inlet and exit pressure of the optimized S-CO_2 RC configuration.

$$\kappa_{diff-vol} = \frac{P_{o3} - P_{o6}}{P_{o3}} \tag{7}$$

As a design choice, the ratio of the absolute meridional velocity at the outlet and the inlet of the impeller is kept equal to 1.375. This number is selected by varying the ratio for the impeller and observing the satisfactory values of exit total thermodynamic conditions using the design algorithm presented in the current section.

For the present study, performance parameters such as the slip factor is adopted from Weisner's correlation **[24]**, as depicted in Equation 8. The distortion factor, λ is another performance parameter, calculated using the expression adopted from Aungier **[21]**.

$$\sigma_{weisner} = 1 - \frac{\sqrt{\sin(\beta_3)}}{z^{0.7}} \tag{8}$$

To initialize the solution, performance parameters such as slip and distortion factors are assumed to be 1 while the losses are assumed to be zero. The Euler turbine equation is used to calculate C_{w3} at the exit of the impeller. Using the tangential velocity, the slip factor correlation is used to calculate the relative flow angle β_3, and the velocity triangle at station 3 is subsequently solved. The blade exit angle β_3 is set equal to the relative flow angle at the impeller exit. The continuity equation is used to calculate the blade height at the impeller exit. Thus, the geometry of the impeller is completely defined. Subsequently, the performance analysis code of the impeller is executed, with the geometrical parameters calculated previously as input to the code. The performance analysis code calculates the exit static pressure and performance parameters such as slip and distortion factors which are updated in the design process and iterated to achieve convergence. Once, the solution is obtained, the isentropic efficiency of the impeller is calculated and further updated leading to an external iterative loop. Finally, the converged

value of isentropic efficiency is obtained. Algorithm of impeller design methodology is depicted in Figure 9.

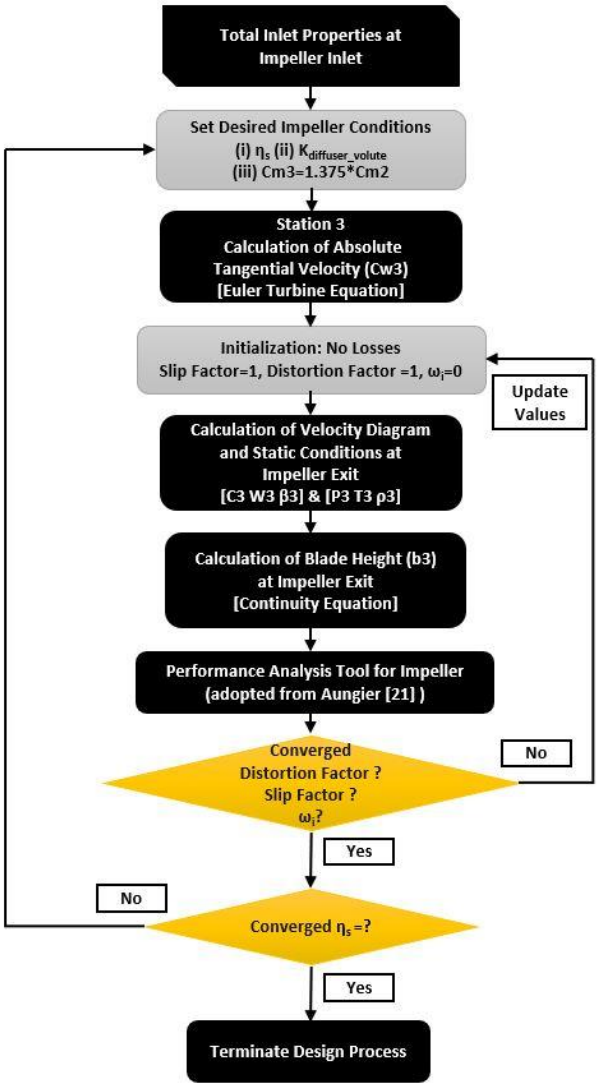

Figure 9: Algorithm for the Impeller Design

DESIGN RESULTS

The geometrical details of the S-CO_2 centrifugal compressor obtained through the inverse design methodology are presented in this section. Certain geometrical parameters are assumed based on prior design experience and are constant throughout the design process. These parameters, with their chosen values, are presented in Table 7.

The calculated geometry of the impeller is presented in Table 8. Note that some parameters are obtained by solving the inverse problem while others are calculated from empirical correlations. Using the values provided in Table 8, two Bezier curves are fitted at the hub and shroud of the impeller to define the flow path of the compressor. Figure 10 shows the schematic of the S-CO_2 impeller with the calculated geometry.

Table 7: Input Geometrical Parameters for Impeller Design

Number of Full Blades	12
Number of Splitter Blades	0
Blade Thickness at Impeller Leading Edge	1 mm
Blade Thickness at Impeller Trailing Edge	1 mm
Clearance Gap between the Shroud and Blade	0.25mm

Table 8: Calculated Geometry of the S-CO_2 Impeller

Impeller Geometry (calculated from design code)	Value
Impeller Inlet Radius at Hub	7.525 mm
Impeller Inlet Radius at Shroud	21.5 mm
Impeller Exit Tip Radius	50 mm
Blade Angle of the Impeller Leading Edge (at Mean Radius)	46.44˚
Blade Angle of the Impeller Trailing Edge	-11.74˚ (backward)
Angle between Streamline and Shaft at Impeller Inlet	0˚
Angle between Streamline and Shaft at Impeller Exit	90˚
Axial Length of the Impeller	38.7 mm
Full Length of the Impeller Blade	68.0 mm
Blade Height at Impeller Inlet	13.725 mm
Blade Height at Impeller Exit	2.6 mm

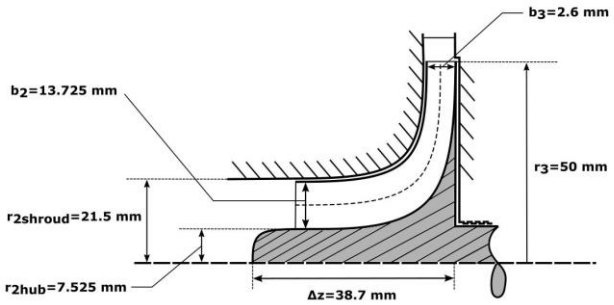

Figure 10: Calculated Geometrical Parameters of the Impeller

Solutions of the velocity triangles at different stations are depicted using velocity triangles presented in Figure 11 and 12. First, it should be noted that all the velocities are subsonic. Secondly, the negative relative angle at the impeller exit implies that the blade is backswept. The absolute velocity angle, α is also slightly on the higher side, which would result into a higher leading-edge blade angle of the diffuser.

A comparison of the desired performance of the centrifugal compressor to the resulting performance from the 1D mean-line analysis code is presented in Table 9. Error in the desired and actual value of exit total pressure is ~ 4%. Thermodynamic

parameters such as the total temperature, enthalpy and entropy have deviations less than 0.3% from the desired values. The density is quite sensitive to change in thermodynamic properties in the supercritical zone, resulting in an error of 1%. For all practical purposes, the performance of the impeller seems to be satisfactory.

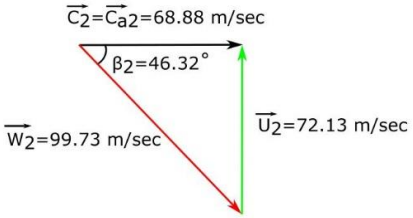

Figure 11: Velocity Triangle at Impeller Inlet

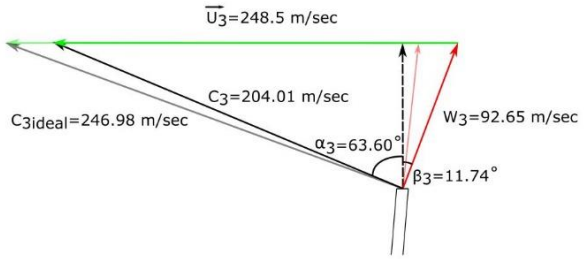

Figure 12: Velocity Triangle at Impeller Exit

Table 9: Performance Comparison of the S-CO_2 Impeller with the Optimized Cycle Parameters

Thermodynamic Properties at Impeller Exit (at mean radius)	Desired Value (From Cycle Optimization)	Calculated Value (From 1D Mean-line Analysis Code)	Deviation (%)
P_o (bar)	307.59	319.44	3.85
T_o (K)	359.16	359.93	0.22
h_o (kJ/kg)	361.86	361.81	0.01
ρ_o (kg/m^3)	736.67	728.06	1.10
S (kJ/kg-K)	1.412	1.410	0.14

For the designed S-CO_2 impeller, the converged isentropic efficiency is reported as 70.07%. This value is very close to the desired value of the compressor, which was fixed during the cycle optimization process as well as an initial guess for the compressor design. The slip factor the S-CO_2 impeller comes out to be 0.826 while the value distortion factor is reported to be 1.389.

CONCLUSIONS

This investigation focused on obtaining the geometrical parameters of a centrifugal compressor for a S-CO_2 cycle using a preliminary one-dimensional design technique. It is found that for the pre-defined heat source, S-CO_2 RC configuration outperforms the RRC configuration. Further, using the method of genetic algorithms, the cycle is optimized and the inlet and exit thermodynamic states of the compressor are defined.

The RRC configuration tends to approach the RC configuration for low heat inputs, as observed in the present study. Along with the identification of range of pressures where the maximum power output is obtained, material constraints is an important aspect that needs to be looked at while selecting and designing components. In the current study, the higher side pressure is restricted by the current heat exchanger technology utilized for S-CO_2 cycles.

Operating close to the critical point is advantageous for the cycle as the net power input to the compressor is reduced. However, close to the critical point, it is likely that the flow accelerates into the two-phase zone. This is a major cause of instability in the code as two-phase is not handled by the currently developed code. A robust model should accommodate handling of two-phase flow during a simulation. A brief condensation analysis ensures that the throat section of the compressor which is more prone to formation of liquid remains free of any condensation.

In addition to modelling of the two-phase fluid, a complete design process includes more practices to fully develop a working compressor. First, the compressor design is completed once all sections, such as the diffuser and volute are defined. The current study focuses only on the inducer and impeller design, and therefore, design of the diffuser and volute models are to be included. Additionally, a CAD model of the compressor is to be generated and a CFD study is to be performed to analyze the performance of the compressor.

NOMENCLATURE

Roman Symbols

A	Annular Area
a	Speed of Sound
b	Blade Height
C	Absolute Velocity
D_s	Specific Diameter
d	Diameter
h	Specific Enthalpy
K	Total Loss in Diffuser and Volute
M	Mach Number
$\dot{m}$	Mass Flow Rate
N_s	Specific Speed
P	Pressure
r	Radius
S	Entropy
s	Fractional Pressure Drop
T	Temperature
t	Blade Thickness
U	Rotational Speed
W	Relative Velocity
$\dot{W}$	Power
z	Number of Blades

Greek Symbol

α	Absolute Flow Angle
β	Relative Flow Angle
Δ	Change
η	Efficiency
π_c	Pressure Ratio
ρ	Density
σ	Slip Factor
τ	Shear Stress Limit
ω	Angular Velocity
$\bar{\omega}$	Total Pressure Loss Coefficient

Subscripts and Superscripts

o	Total or Stagnation State
a	Value at Actual State
m	Meridional Component
s	Value for Isentropic Process
sat	Saturated Condition
th	Throat
$turb$	Turbine
U	Tangential Component
$\bar{x}$	Mean Value of x
$\vec{x}$	Vector x

Abbreviations

LTR	Low Temperature Recuperator
HTR	High Temperature Recuperator
MTPA	Million Tons Per Annum
RC	Recuperated Cycle
RRC	Re-compressed Recuperated Cycle
S-CO_2	Supercritical Carbon dioxide
WHR	Waste Heat Recovery

REFERENCES

[1] IEA (2019), World Energy Outlook 2019, IEA, Paris, https://www.iea.org/reports/world-energy-outlook-2019

[2] Johnson, Ilona, Choate, William T., and Davidson, Amber. *Waste Heat Recovery Technology and Opportunities in U.S. Industry*. United States: N. p., 2008. Web. doi:10.2172/1218716.

[3] Naik-Dhungel, Neeharika, 2012, "WASTE HEAT TO POWER SYSTEMS", Combined Heat and Power Partnership, U.S. Environmental Protection Agency.

[4] Sulzer, 1948, "Verfahren zur Erzeugung von Arbeit aus Warme," Swiss Patent: 269 599.

[5] Feher, E. G., 1968, "The Supercritical Thermodynamic Power Cycle," Energy Conversion, 8(2), pp. 85–90

[6] Angelino, G., 1968, "Carbon Dioxide Condensation Cycles," J. Eng. Power, Julio, pp. 287–295.

[7] Lettieri, C., Yang, D., and Spakovszky, Z., 2015, "An Investigation of Condensation Effects in Supercritical Carbon Dioxide Compressors," J. Eng. Gas Turbines Power, 137(8), pp. 1–8.

[8] Wright, S. A., Davidson, C. S., and Scammell, W. O., 2016, "Thermo-Economic Analysis of Four SCO_2 Waste Heat Recovery Power Systems," 5th Int. Symp. - Supercrit. CO_2 Power Cycles, pp. 1–16.

[9] Khurana, S., Banerjee, R. and Gaitonde, U., 2002, "Energy balance and cogeneration for a cement plant," *Applied thermal engineering*, *22*(5), pp.485-494.

[10] MATLAB, 2010. version 9.4.0.813654 (R2018a), Natick, Massachusetts: The MathWorks Inc.

[11] Bell, I.H., Wronski, J., Quoilin, S. and Lemort, V., 2014, "Pure and pseudo-pure fluid thermophysical property evaluation and the open-source thermophysical property library CoolProp," *Industrial & engineering chemistry research*, *53*(6), pp.2498-2508.

[12] Mohagheghi, M., and Kapat, J., 2013, "Thermodynamic Optimization of Recuperated S-CO_2 Brayton Cycles for Waste Heat Recovery Applications," 4th Int. Symp. - Supercrit. CO_2 Power Cycles, 53(9), pp. 1689–1699.

[13] Khadse, A., Blanchette, L., Kapat, J., Vasu, S., Hossain, J., and Donazzolo, A., 2018, "Optimization of Supercritical CO_2 Brayton Cycle for Simple Cycle Gas Turbines Exhaust Heat Recovery Using Genetic Algorithm," J. Sol. Energy Eng. Trans. ASME, 140(7).

[14] Mitchell, M., 1998, "An Introduction to Genetic Algorithms (Complex Adaptive Systems)," MIT Press.

[15] Fleming, D., Holschuh, T., Conboy, T., Rochau, G., and Fuller, R., 2012, "Scaling Considerations for a Multi-Megawatt Class Supercritical CO_2 Brayton Cycle and Path Forward for Commercialization," pp. 953–960.

[16] Balje, O. E., 1981, "Turbomachines. A Guide to Design, Selection and Theory."

[17] Fuller, R., Preuss, J., and Noall, J., 2012, "Turbomachinery for Supercritical CO_2 Power Cycles," pp. 961–966.

[18] Monje, B., Sánchez, D., Savill, M., Pilidis, P., and Sánchez, T., 2014, "A Design Strategy for Supercritical CO_2 Compressors," Proc. ASME T.E., 3B, pp. 1–11.

[19] Loewenthal, S. H., 1984, "Design of Power-Transmitting Shafts.," NASA Ref. Publ.

[20] Dowson, P., Bauer, D., and Laney, S., 2008, "Selection of Materials and Material Related Processes for Centrifugal Compressors and Steam Turbines in the Oil and Petrochemical Industry," Proc. thirty-seventh Turbomachinery Symposium.

[21] Aungier, R. H., 2000, "Centrifugal Compressors: A Strategy for Aerodynamic Design and Analysis," ASME Press.

[22] Wright, S. a, Radel, R. F., Vernon, M. E., Rochau, G. E., and Pickard, P. S., 2010, "Operation and Analysis of a Supercritical CO2 Brayton Cycle," SANDIA Rep. SAND2010-0171, (September), p. 101.

[23] Vilim, R. B., 2010, "A One-Dimensional Compressor Model for Super-Critical Carbon Dioxide Applications," *International Congress on Advances in Nuclear Power Plants 2010, ICAPP 2010*.

[24] Wiesner, F. J., 1967, "A Review of Slip Factors for Centrifugal Impellers," J. Eng. Gas Turbines Power, **89**(4), pp. 558–566.

DOI: 10.17185/duepublico/73958
URN: urn:nbn:de:hbz:464-20210330-103937-1